Higher order forward spin polarizability

B. Pasquini[a,b], P. Pedroni[b], D. Drechsel[c]

[a]*Dipartimento di Fisica Nucleare e Teorica,*

Università degli Studi di Pavia, Pavia, Italy

[b]*Istituto Nazionale di Fisica Nucleare,*

Sezione di Pavia, Pavia, Italy

[c]*Institut für Kernphysik,*

Johannes Gutenberg Universität,

D-55099 Mainz, Germany

As a guideline for future experiments to extract the four (leading) spin polarizabilities of the nucleon, we have constructed the forward amplitude for polarized Compton scattering by dispersion integrals. These integrals have been saturated by recently measured helicity-dependent photoabsorption cross sections as well as predictions for pion photoproduction multipoles from several phenomenological descriptions and chiral perturbation theory. The comparison of these results corroborates the strategy to extract the spin polarizabilities by fitting them to polarized Compton data and fixing all higher order spin effects by dispersion relations based on pion photoproduction multipoles.

I.   INTRODUCTION

Real Compton scattering (RCS) probes the response of a complex system to an external electromagnetic field. In particular, photon scattering off the nucleon is described by six independent helicity amplitudes depending on the lab energy E_γ and the scattering angle θ of the photon. The low-energy expansion (LEX) of these amplitudes defines two spin-independent (scalar) and four spin-dependent (vector) polarizabilities, appearing at order E_γ^2 and E_γ^3, respectively. These polarizabilities are fundamental structure constants of the nucleon just as its size and shape.

Whereas the scalar polarizabilities have been measured quite accurately by comparing the RCS data directly to the LEX [1, 2], the quest to determine the vector polarizabilities is still going on. The difficulty to measure the vector polarizabilities is caused by their suppression at low energies, which makes it impossible to extract them at energies $E_\gamma < 100$ MeV. With increasing energies, on the other hand, the LEX converges slower and slower and finally breaks down at pion-production threshold, $E_\gamma = m_\pi + m_\pi^2/(2M) \approx 150$ MeV, where m_π and M are the pion and nucleon masses, respectively. In order to determine the vector polarizabilities from RCS data, it is prerequisite to (i) analyze the data within a theoretical framework covering the energy region up to the $\Delta(1232)$ resonance at $E_\gamma \approx 300$ MeV and (ii) perform dedicated experiments with polarized photons and nucleons with increased sensitivity to the spin-dependent amplitudes.

The sensitivity of various single and double polarization observables to the spin polarizabilities has been studied by subtracted dispersion relations based on the pion photoproduction multipoles [3]. The authors concluded that a complete separation of the polarizabilities should be possible by dedicated polarization experiments between pion threshold and the $\Delta(1232)$ region, provided that polarization measurements can be achieved within an accuracy of a few percent. Such an experiment to extract the spin polarizabilities has recently been proposed at MAMI [4].

The predictions of chiral perturbation theory (ChPT) at $\mathcal{O}(p^4)$ are in good agreement with the empirical data for the scalar polarizabilities of the proton [5]. However, in order to cover the energy region necessary for the extraction of the vector polarizabilities, the $\Delta(1232)$ must be included as a dynamic degree of freedom [6–9].

Recently, these polarizabilities have also been studied in lattice QCD. The first results for

the magnetic polarizability of the proton are quite encouraging [10], whereas quite different values are reported for the electric polarizability [11–16]. It was also proposed to extract the spin polarizabilities from lattice calculations [17]. However, calculations with dynamic and lighter quarks are prerequisite to extrapolate to the physical point in a reliable way, because these polarizabilities show distinct signatures of chiral dynamics [7].

As stated above, the complete separation of the six polarizabilities of the nucleon requires both new polarization data and a theoretical framework for RCS, which will necessarily contain some model dependence through parameters describing the high-energy regime. Such parameters are the low-energy constants appearing in ChPT, and in dispersion relations the extrapolation of the photoproduction data to regions not covered by the experiment. Any additional confirmation of the theoretical framework by independent experimental information is therefore most welcome. On that ground it is the aim of the present work to construct the full spin-dependent RCS amplitude in forward direction from data given by (helicity-dependent) total photoabsorption cross sections. In Sec. II we present the formalism necessary to discuss the forward scattering amplitudes and their relations to dispersion integrals over inclusive photoabsorption cross sections, the LEX defining the leading and higher order forward spin polarizabilities (FSPs) as well as the "dynamic" FSP describing the full spin-dependent response to forward scattering. The relevant dispersion integrals are evaluated in Sec. III and compared with several model predictions. Finally, we conclude with a brief section summarizing our findings.

II. KINEMATICS, AMPLITUDES, AND SPIN POLARIZABILITIES

The polarizability of the nucleon is determined by Compton scattering [18, 19],

$$\gamma(k) + N(p) \rightarrow \gamma(k') + N(p'),\tag{1}$$

where k and p denote the momentum four-vectors of the incoming photon and nucleon, respectively, with the primed quantities standing for the final state momenta. Compton scattering can be described by the two Lorentz invariants $\nu = K \cdot P/M$ and $t = (k - k')^2$, with $K = (k+k')/2$ and $P = (p+p')/2$. These invariants are related to the initial (E_γ) and

final (E'_γ) photon laboratory energies, and to the laboratory scattering angle θ_{lab} by

$$t = -4E_\gamma E'_\gamma \sin^2 \frac{\theta_{\text{lab}}}{2} = -2M(E_\gamma - E'_\gamma) \, ,$$
$$\nu = E_\gamma + \frac{t}{4M} = \frac{1}{2}(E_\gamma + E'_\gamma). \tag{2}$$

In the forward direction, the invariants take the values

$$\nu = E_\gamma = E'_\gamma \, , \quad t = 0. \tag{3}$$

For the theoretical calculations of Compton scattering it is convenient to use the center-of momentum (c.m.) system. With ω and ω' the photon c.m. energies in the initial and final states, respectively, and $\omega = \omega'$, the analog of Eq. (3) in the c.m. frame is

$$\nu = \omega(\sqrt{1 + \omega^2/M^2} + \omega/M) \, , \quad t = 0. \tag{4}$$

The forward Compton amplitude takes the form

$$T(\nu, \theta = 0) = \vec{\varepsilon}'^* \cdot \vec{\varepsilon} \, f(\nu) + i\, \vec{\sigma} \cdot (\vec{\varepsilon}'^* \times \vec{\varepsilon}) \, g(\nu) \, , \tag{5}$$

where $\vec{\varepsilon}$ and $\vec{\varepsilon}'$ are the photon polarizations in the initial and final states, respectively, and $\vec{\sigma}$ is the spin operator of the nucleon. Because of the crossing symmetry, the amplitude T is invariant under the transformation $\vec{\varepsilon} \to \vec{\varepsilon}'$ and $\nu \to -\nu$. As a result, f is an even and g an odd function of ν.

The amplitudes f and g can be determined by scattering circularly polarized photons (e.g., helicity $\lambda = 1$) off nucleons polarized along or opposite to the photon momentum $\vec{k}$. Depending on the relative orientation of the spins, the absorption of the photon leads to hadronic excited states with spin projections $1/2$ or $3/2$. The optical theorem expresses the unitarity of the scattering matrix by relating the respective absorption cross sections, $\sigma_{1/2}$ and $\sigma_{3/2}$, to the imaginary parts of the forward scattering amplitudes,

$$\text{Im } f(\nu) = \frac{\nu}{8\pi} \left(\sigma_{1/2}(\nu) + \sigma_{3/2}(\nu) \right) \, ,$$
$$\text{Im } g(\nu) = \frac{\nu}{8\pi} \left(\sigma_{1/2}(\nu) - \sigma_{3/2}(\nu) \right) . \tag{6}$$

In the following, we restrict the discussion to the spin-dependent amplitude $g(\nu)$. Using causality, the crossing symmetry, the optical theorem and an appropriate high-energy behavior of the scattering amplitude, we may set up the following unsubtracted dispersion

relation:

$$\text{Re } g(\nu) = \frac{\nu}{4\pi^2} \mathcal{P} \int_{\nu_0}^{\infty} \frac{\sigma_{1/2}(\nu') - \sigma_{3/2}(\nu')}{\nu'^2 - \nu^2} \nu' d\nu' \,, \tag{7}$$

where $\nu_0 = m_\pi + m_\pi^2/(2M)$ is the threshold for producing a pion with mass m_π. If the integral exists, it has a Taylor series expansion about $\nu = 0$, with a convergence radius given by the onset of inelasticities at ν_0. This series can be compared to the LEX of the spin-flip amplitude [19],

$$g(\nu) = -\frac{e^2 \kappa_N^2}{8\pi M^2} \nu + \gamma_0 \nu^3 + \bar{\gamma}_0 \nu^5 + \mathcal{O}(\nu^7). \tag{8}$$

The leading term of this expansion is due to intermediate nucleon states (Born terms). The comparison of the LEX with the Taylor expansion of Eq. (7) yields the Gerasimov-Drell-Hearn (GDH) relation between the anomalous magnetic moment of the nucleon, κ_N, and the spin-dependent absorption spectrum,

$$\frac{\pi e^2 \kappa_N^2}{2M^2} = \int_{\nu_0}^{\infty} \frac{\sigma_{3/2}(\nu') - \sigma_{1/2}(\nu')}{\nu'} d\nu' \equiv I_{\text{GDH}}. \tag{9}$$

The higher-order terms are produced by the hadronic excitation spectrum (non-Born or dispersive contributions). These terms parameterize the FSPs of the nucleon. In particular, the leading and next-to-leading FSPs are given by

$$\begin{aligned}
\gamma_0 &= \frac{1}{4\pi^2} \int_{\nu_0}^{\infty} \frac{\sigma_{1/2}(\nu') - \sigma_{3/2}(\nu')}{\nu'^3} d\nu' \,, \\
\bar{\gamma}_0 &= \frac{1}{4\pi^2} \int_{\nu_0}^{\infty} \frac{\sigma_{1/2}(\nu') - \sigma_{3/2}(\nu')}{\nu'^5} d\nu' \,.
\end{aligned} \tag{10}$$

Furthermore, we may define the crossing-even "dynamic" FSP $\gamma_0^{\text{dyn}}(\nu)$ by

$$\begin{aligned}
g(\nu) &= -\frac{e^2 \kappa_N^2}{8\pi M^2} \nu + \gamma_0^{\text{dyn}}(\nu) \nu^3 \,, \\
\text{Re}[\gamma_0^{\text{dyn}}(\nu)] &= \frac{1}{4\pi^2} \mathcal{P} \int_{\nu_0}^{\infty} \frac{\sigma_{1/2}(\nu') - \sigma_{3/2}(\nu')}{\nu'(\nu'^2 - \nu^2)} d\nu' \,, \\
\text{Im}[\gamma_0^{\text{dyn}}(\nu)] &= \frac{\sigma_{1/2}(\nu) - \sigma_{3/2}(\nu)}{8\pi\nu^2} \,.
\end{aligned} \tag{11}$$

For $\nu < \nu_0$ the imaginary part vanishes, and the "dynamic" FSP has the following LEX:

$$\gamma_0^{\text{dyn}}(\nu) = \gamma_0 + \bar{\gamma}_0 \nu^2 + \mathcal{O}(\nu^4). \tag{12}$$

In comparing with the literature, we note that the expression "dynamic polarizability" in Refs. [7] and [19] refers to the energy dependence of the polarizability due to individual

electromagnetic multipole radiation or combinations thereof. On the other hand, the FSP $\gamma_0^{\mathrm{dyn}}(\nu)$ of Eq. (11) describes the nucleon's forward spin response to the full electromagnetic field, including the contributions of all the multipoles and their retardation.

The general theory of Compton scattering involves 6 crossing-even amplitudes $A_i(\nu, t)$ describing the dispersive part of the scattering matrix [18, 19]. In particular, the forward scattering amplitude g is related to A_4 as follows:

$$A_4(\nu, t = 0) = \frac{2\pi M}{\nu^3}\left(g(\nu) - \nu g'(0)\right). \tag{13}$$

Using Eqs. (11) - (13) we may cast the polarizabilities into the form

$$\gamma_0 = \frac{a_4}{2\pi M}, \quad \bar{\gamma}_0 = \frac{a_{4,\nu}}{2\pi M}, \tag{14}$$

with

$$a_4 = A_4(0, 0), \quad a_{4,\nu} = \frac{\partial}{\partial \nu^2} A_4(\nu, 0)|_{\nu=0}. \tag{15}$$

If the invariant ν is expressed by the c.m. energy ω according to Eq. (4), the LEX of Eq. (8) takes the form

$$g(\omega) = -\frac{e^2 \kappa_N^2}{8\pi M^2}\omega(1 + \frac{\omega}{M} + \frac{\omega^2}{2M^2} - \frac{\omega^4}{8M^4})$$
$$+ \gamma_0 \omega^3(1 + \frac{3\omega}{M} + \frac{9\omega^2}{2M^2}) + \bar{\gamma}_0 \omega^5 + \mathcal{O}(\omega^6). \tag{16}$$

We observe that the nucleon Born term, proportional to κ_N^2, contributes a series of recoil terms in ω/M. The remaining dispersive terms contain the spin polarizabilities related to the excited states of the nucleon. As for the ν expansion, the spin polarizability γ_0 appears as coefficient of the third order term, now in ω^3. In addition, however, γ_0 appears also with recoil terms of order ω^4 and ω^5. Combining all the ω^5 dispersive terms to $\tilde{\gamma}_0 \omega^5$, we find the relation

$$\tilde{\gamma}_0 = \bar{\gamma}_0 + \frac{9}{2M^2}\gamma_0. \tag{17}$$

According to Ref. [20], the $\mathcal{O}(\omega^3)$ and $\mathcal{O}(\omega^5)$ FSPs have the following multipole decomposition:

$$\gamma_0 = -(\gamma_{E1E1} + \gamma_{M1M1} + \gamma_{M1E2} + \gamma_{E1M2}), \tag{18}$$

$$\tilde{\gamma}_0 = -(\gamma_{E1E1\nu} + \gamma_{M1M1\nu} + \gamma_{M1E2\nu} + \gamma_{E1M2\nu}$$
$$+ \gamma_{E2E2} + \gamma_{M2M2} + \frac{8}{5}\gamma_{E2M3} + \frac{8}{5}\gamma_{M2E3}). \tag{19}$$

In Eq. (19), the first row contains retardation corrections related to the leading FSP, whereas the second row shows higher multipole structures probing the quadrupole and octupole excitation of the system. We note that the above multipole notation of Ref. [19] is related to the nomenclature of Ref. [20] as follows:

$$\gamma_{E1E1} = \gamma_{E1}, \quad \gamma_{M1M1} = \gamma_{M1},$$
$$\gamma_{M1E2} = \gamma_{E2}, \quad \gamma_{E1M2} = \gamma_{M2},$$
$$\gamma_{E2E2} = \gamma_{ET}, \quad \gamma_{M2M2} = \gamma_{MT},$$
$$\gamma_{E2M3} = \gamma_{M3}, \quad \gamma_{M2E3} = \gamma_{E3}. \tag{20}$$

III.   RESULTS FOR THE GDH SUM RULE AND THE FORWARD SPIN POLARIZABILITIES

A.   Evaluation of the dispersion integrals

The dispersion integrals defined in Eqs. (9) and (10) were evaluated using the data obtained by the GDH collaboration at the MAMI (Mainz) and ELSA (Bonn) tagged photon facilities. The contributions of kinematical regions not covered by the data were determined on the basis of various multipole analyses for pion photoproduction, with systematic errors estimated by comparison of different model predictions. In particular, we used the work of Hanstein *et al.* (HDT) based on dispersion relations [21], the recent version of the SAID09 multipole analysis [22], the unitary isobar model MAID07 [23], the dynamical DMT model [24], and the predictions of heavy baryon chiral perturbation theory (HBChPT) according to Ref. [20].

The experimental data base includes:

- the helicity-dependent differential cross section $[(\mathrm{d}\sigma/\mathrm{d}\Omega)_{3/2} - (\mathrm{d}\sigma/\mathrm{d}\Omega)_{1/2}]$ data for the $n\pi^+$ channel measured at $E_\gamma = (0.18 \pm 0.005)$ GeV and $E_\gamma = (0.19 \pm 0.005)$ GeV in the angular range $45° \leq \theta^* \leq 109°$, where θ^* is the pion emission angle in the c.m. frame [25],

- the helicity-dependent data for the total inclusive cross section, $\Delta\sigma = \sigma_{1/2} - \sigma_{3/2}$, starting at $E_\gamma = (0.204 \pm 0.009)$ GeV and extending to $E_\gamma = (2.82 \pm 0.09)$ GeV [26–28].
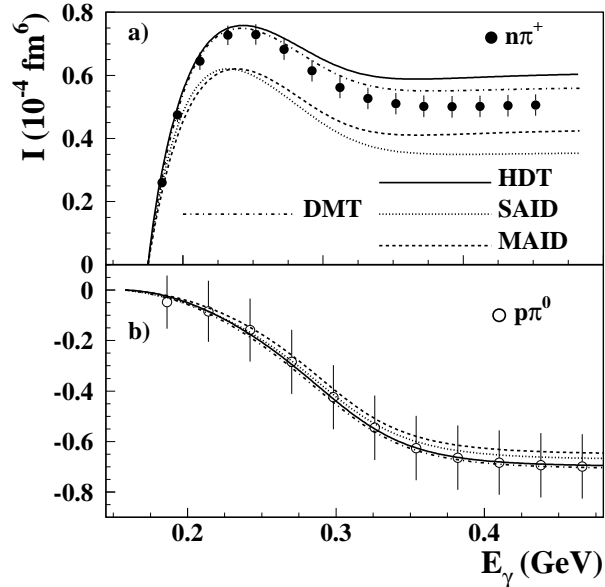
FIG. 1: The experimental running integrals $I(E_\gamma)$ of Eq. (21) as obtained from the data of the GDH Collaboration [25] compared to the HDT [21], SAID09 [22], MAID07 [23], and DMT [24] predictions. The top and bottom panels display the contributions of the $n\pi^+$ and $p\pi^0$ channels, respectively. For both the experimental and the theoretical values, the integration starts at the lowest measured photon energy $E_{\gamma,\text{min}}$, that is, 0.175 GeV fo $n\pi^+$ and 0.158 GeV for $p\pi^0$. Only the statistical errors are shown.

As a first step to evaluate the dispersion integrals, the data at $E_\gamma = (0.18 \pm 0.005)$ GeV and $E_\gamma = (0.19 \pm 0.005)$ GeV were used to obtain the $n\pi^+$ contribution to $\Delta\sigma$ at these energies and in the measured angular range. The extrapolation into the unmeasured region of θ^* was performed with the HDT analysis which reproduces the experimental data for $E_\gamma \leq 0.3$ GeV quite well, see for example Fig. 7 of Ref. [25]. The error associated with this extrapolation was estimated by comparison with the SAID09, MAID07, and DMT multipole analyses. As a result we found an absolute systematic error of about $\pm 5\%$ for the calculated total cross section value. In order to check the validity of this estimation, we evaluated the experimental "running integral" I for the FSP $\bar{\gamma}_0$,

$$I(E_\gamma) = \frac{1}{4\pi^2} \int_{E_{\gamma,\text{min}}}^{E_\gamma} \frac{\sigma_{1/2}(\nu) - \sigma_{3/2}(\nu)}{\nu^5}\, d\nu \,, \tag{21}$$

where the lower integration limit $E_{\gamma,\text{min}}$ corresponds to the lowest measured photon-energy bin and the upper integration limit is taken as the running variable.

Figure 1a) shows the data points based on (i) our evaluation of the helicity dependent $n\pi^+$ total cross section data in the energy range $0.175\,\text{GeV} \leq E_\gamma \leq 0.195\,\text{GeV}$ [25] and (ii) the published helicity-dependent $n\pi^+$ total cross section data in the energy range $0.195\,\text{GeV} \leq E_\gamma \leq 0.450\,\text{GeV}$ [25]. The data are compared with the predictions of four multipole analyses as indicated in the figure. The good agreement between the experimental data and the results of the HDT and DMT models for $E_\gamma < 250\,\text{MeV}$ gives reasonable confidence in our extrapolation to the lower energies. However, the $1/\nu^5$ weight in the integrand of Eq. (21) clearly enhances the contribution of the unmeasured threshold region relative to the high energy region. In performing the integrals, it is also important to consider the isospin breaking effects, at least via the pion mass splitting. The pion masses used in our extrapolation to threshold are $m_{\pi^0} = 134.98\,\text{MeV}$ and $m_{\pi^\pm} = 139.57\,\text{MeV}$ for the neutral and charged pions, respectively. The results for the $\gamma p \to p\pi^0$ channel are shown in Fig. 1b) by comparison of the multipole predictions with the helicity-dependent data in the range from $E_\gamma = (0.172 \pm 0.014)\,\text{GeV}$ to $E_\gamma = 0.45\,\text{GeV}$ [25]. Because the measured $p\pi^0$ data point below 0.2 GeV gives only a very small contribution to the integrals but have a large statistical error, we choose to evaluate the $p\pi^0$ contribution of this energy range with the HDT analysis. This choice minimizes the overall (statistical+systematic) error related to the integral evaluation.

Concerning the unmeasured contribution of the $\gamma p \to n\pi^+$ channel below 0.175 GeV, we observe that the S-wave multipole E_{0+} plays an overwhelming role in the threshold region. An accurate knowledge of this multipole is mandatory in order to obtain a reliable estimate of this low-energy contribution. Fortunately, the value of E_{0+} at threshold is known rather precisely through the low-energy theorem for charged pion photoproduction. However, current predictions differ with respect to the slope of E_{0+} in the threshold region. Figure 2 displays the contribution of the E_{0+} multipole for the $n\pi^+$ channel to the helicity-dependent cross section $\Delta\sigma$ in the threshold region. The results according to HDT, SAID09, MAID07, and DMT are compared to the analysis of Ref. [29]. The latter work extends the results of low-energy theorems for threshold pion photoproduction within the framework of HBChPT by fitting the unknown low-energy constants appearing at $\mathcal{O}(p^3)$ to data on radiative pion capture [30] and pion photoproduction [31].

Figure 2 shows that the predictions are in good agreement for $E_\gamma \leq 0.175\,\text{GeV}$ except for the MAID results. The different behavior of MAID is due to the fact that the unitarization
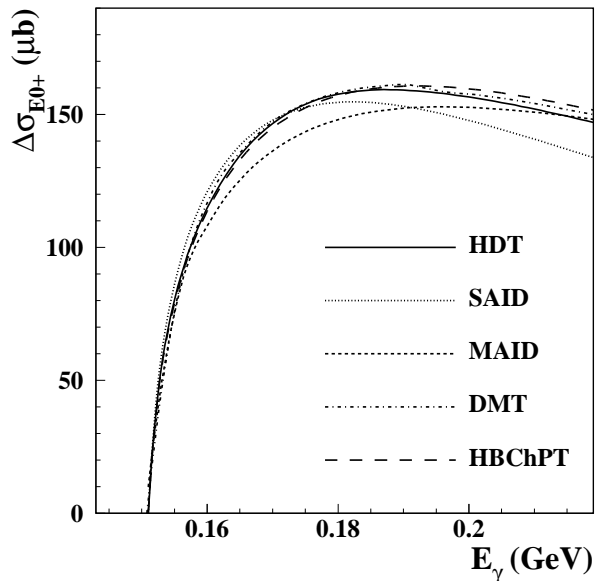
FIG. 2: The contribution of the E_{0+} multipole for the charged-pion channel to $\Delta\sigma = (\sigma_{1/2} - \sigma_{3/2})$ obtained from the HDT [21], SAID09 [22], MAID07 [23], and DMT [24] analyses as well as the predictions of HBChPT [29].

involving the $S_{11}(1535)$ resonance underestimates the size of pion rescattering near threshold. We have therefore evaluated the contribution of the $n\pi^+$ channel below $E_\gamma = 175$ MeV using the HDT multipoles. The associated systematic error has been estimated by comparison with the predictions of the other models excluding MAID.

B. Discussion of the results

Table I summarizes the measured and evaluated contributions of the different energy regions to the GDH sum rule, the leading FSP, and the subleading FSP as well as the statistical and systematic errors. Statistical errors are given in standard deviation (sd) units while systematic ones are given in half interval ($\Delta/2$) units. For the GDH sum rule and the leading FSP γ_0, the contributions above 2.91 GeV are taken from the estimates given in Ref. [32], whereas such high-energy contributions can be safely neglected for $\bar{\gamma}_0$.

In Table II we compare our results for the FSPs γ_0 and $\bar{\gamma}_0$ to (i) predictions obtained in HBChPT at $\mathcal{O}(p^3)$ and at $\mathcal{O}(\epsilon^3)$ in the small scale expansion (SSE) including the $\Delta(1232)$

channel	energy (GeV)	GDH (μb)	stat. (sd)	syst. ($\Delta/2$)	γ_0 (10^{-4} fm^4)	stat. (sd)	syst. ($\Delta/2$)	$\bar{\gamma}_0$ (10^{-4} fm^6)	stat. (sd)	syst. ($\Delta/2$)
$n\pi^+$	≤ 0.175	-16		±1	$+0.56$		±0.01	$+0.83$		±0.02
$p\pi^0$	≤ 0.195	1		±0.1	-0.03		±0.05	-0.04		±0.01
$n\pi^+$	$0.175 - 0.195$	-14	±1	±1	$+0.40$	±0.02	±0.02	$+0.46$	±0.02	±0.02
$\gamma p \to X$	$0.195 - 2.91$	253	±6	±13	-1.85	±0.07	±0.05	-0.65	±0.07	±0.05
$\gamma p \to X$	> 2.91	-14		±2	0.01					
total		210	±6	±14	-0.90	±0.08	±0.11	$+0.60$	±0.07	±0.07

TABLE I: Contributions from different photon energy regions to the GDH integral I_{GDH}, the leading FSP γ_0, and the subleading FSP $\bar{\gamma}_0$ defined by Eqs. (9) and (10) as well as the associated statistical and systematic errors. The GDH sum rule predicts 204 μb. See text for further information.

	γ_0 (10^{-4} fm^4)	$\bar{\gamma}_0$ (10^{-4} fm^6)	$\tilde{\gamma}_0$ (10^{-4} fm^6)	recoil (10^{-4} fm^6)
$\mathcal{O}(p^3)$ [20]	4.6	4.23	5.15	0.92
$\mathcal{O}(\epsilon^3)$ [20]	2.9	3.65	4.23	0.58
dispersion [21]	-0.69	0.69	0.56	-0.14
our evaluation	$-0.90 \pm 0.08 \pm 0.11$	$0.60 \pm 0.07 \pm 0.07$	$0.42 \pm 0.09 \pm 0.09$	$0.18 \pm 0.02 \pm 0.02$

TABLE II: The FSPs of the proton. The leading FSP γ_0 appears as coefficient of the amplitude at third order in both the lab energy ν and the c.m. energy ω. The next-to-leading FSP, $\bar{\gamma}_0$ in the lab system and $\tilde{\gamma}_0$ in the c.m. system, appear at fifth order in the respective energies. They differ by the recoil term given in the last column of the table. The predictions are obtained from HBChPT at $\mathcal{O}(p^3)$ and $\mathcal{O}(\epsilon^3)$ [20] as well as dispersion theory based on the HDT multipoles of the one-pion channels.

as an explicit degree of freedom [20] as well as (ii) results based on dispersion relations using the pion photoproduction multipoles of HDT up to 500 MeV and extended by the SAID multipoles to the higher energies. The FSPs found from our analysis are in good agreement with the results obtained by dispersion relations. However, the FSPs are considerably overestimated by lowest order HBChPT. Further works on the leading spin polarizability γ_0

resulted in the following values (all in units of 10^{-4} fm^4): -3.9 to $\mathcal{O}(p^4)$ in HBChPT [33], 2.0 to $\mathcal{O}(\epsilon^3)$ in SSE [6], and -0.9 at NNLO in manifestly Lorentz-covariant ChPT [34]. The dependence of the dispersive predictions on the one-pion photoproduction multipoles is illustrated in Table III. The solution labeled HDT corresponds to the HDT multipoles as given over the energy range $\nu_0 < E_\gamma < 0.5$ GeV, supplemented by the SAID parametrization for 0.5 GeV $< E_\gamma < 3$ GeV. The MAID07 and SAID09 predictions are obtained from the most recent parameterizations of these models for $\nu_0 < E_\gamma < 3$ GeV. Finally, the solution labeled DMT is based on the DMT multipoles in the range $\nu_0 < E_\gamma < 1.7$ GeV, supplemented by the SAID09 parametrization in the range 1.7 GeV $< E_\gamma < 3$ GeV.

Beyond the one-pion channel, we estimated the contribution from multi-pion intermediate states by inelastic decay of πN resonances as detailed in Ref. [35]. The inelastic contributions are assumed to have the same helicity structure as the one-pion channels. In this approximation, we first calculate the resonant part of the pion photoproduction multipoles using the Breit-Wigner parametrization of Ref. [36] and then scale this contribution by a suitable factor to include the inelastic decay of the resonances. As shown in Table III, this procedure yields a multi-pion contribution of $(20 \pm 2)\,\mu$b to the GDH sum rule. On the other hand, we have evaluated this contribution on the basis of recently published data for the helicity dependence of the $\gamma p \to N\pi\pi$ channels in the energy range 325 MeV $< E_\gamma < 800$ MeV [37–39]. ¿From the data in the limited energy range covered by the experiments, we have obtained a two-pion contribution of $(39 \pm 1 \pm 3)\,\mu$b, about twice the value of the model predictions. The difference between the data and the predictions has its origin in the strong two-pion contribution observed in the energy range $500 < E_\gamma < 700$ MeV, which can not be described by the resonance model. In view of this discrepancy, an improved theoretical description of the multi-pion continuum states is prerequisite to describe the GDH sum rule in a quantitative way. As may be expected from the energy-weight factors in the respective integrals, Table III shows only small multi-pion effects for the FSPs.

Figures 3-5 display the running integrals for the GDH integral I_{GDH}, the leading FSP γ_0 and the subleading FSP $\bar{\gamma}_0$. These integrals are defined as in Eq. (21), with the appropriate weight factors in the denominator. Figure 3 compares our result with the predictions of several multipole analyses. The shaded bands represent the statistical and systematic errors associated with our analysis, which includes both the experimental errors and the model errors of the extrapolation into the unmeasured regions. The model predictions lie within

	GDH (μb)	γ_0 (10^{-4} fm^4)	$\bar{\gamma}_0$ (10^{-4} fm^6)
HDT	177 (196)	$-0.67(-0.69)$	0.69 (0.69)
MAID	163 (182)	$-0.65(-0.67)$	0.65 (0.64)
SAID	191 (208)	$-0.86(-0.88)$	0.57 (0.57)
DMT	185 (205)	$-0.76(-0.78)$	0.64 (0.64)

TABLE III: Results for the GDH sum rule, the leading FSP γ_0, and the subleading FSP $\bar{\gamma}_0$ as obtained from the pion photoproduction multipoles of HDT, MAID, SAID, and DMT. The values in bracket include the multi-pion contributions.

the error bars of our analysis, except for the running GDH integral above 0.5 GeV. In the latter case the model predictions stay below the data by about $30\,\mu$b, mostly because of the missing multi-pion strength.

The multipole decompositions of the $n\pi^+$ and $p\pi^0$ channels are shown in Figs. 4 and 5, respectively. The $n\pi^+$ channel is characterized by a strong competition between the E_{0+} multipole above threshold and the M_{1+} near the $\Delta(1232)$ resonance, whereas the neutral pion channel is almost completely described by $\Delta(1232)$ resonance effects.

The real and imaginary parts of the dynamic FSP γ_0^{dyn}, as defined by Eq. (11), are displayed in Fig. 6. Up to the lowest threshold at $E_\gamma = \nu_0$, the real part can be expanded in a power series according to the LEX, Eq. (12). Of course, the convergence of the series deteriorates with increasing energy. Up to $E_\gamma = 50$ MeV, the forward scattering amplitude is described by the leading polarizability γ_0 within an accuracy of 10%. In order to obtain the same precision at 80 MeV, also $\bar{\gamma}_0$ must be included, and already four terms of the series are necessary at 100 MeV. As shown in Fig. 6, the onset of S-wave pion production at $E_\gamma = \nu_0$ leads to a strong cusp effect in the real part. The rapid increase of the dynamic FSP from its static value $-0.90 \cdot 10^{-4}$ fm^4 at $E_\gamma = 0$ to about $6 \cdot 10^{-4}$ fm^4 at pion threshold clearly shows the necessity to analyze Compton scattering within the framework of dispersion analysis. In particular, such an approach is prerequisite in order to determine the spin polarizabilities, which yield significant contributions to the cross section only for photon energies above 80 MeV. Near $E_\gamma \approx 300$ MeV, the dynamic FSP is dominated by the resonance structure of the $\Delta(1232)$. Except for the minimum of $\mathrm{Re}[\gamma_0^{\mathrm{dyn}}]$ near $E_\gamma = 0.23$ GeV, our analysis is
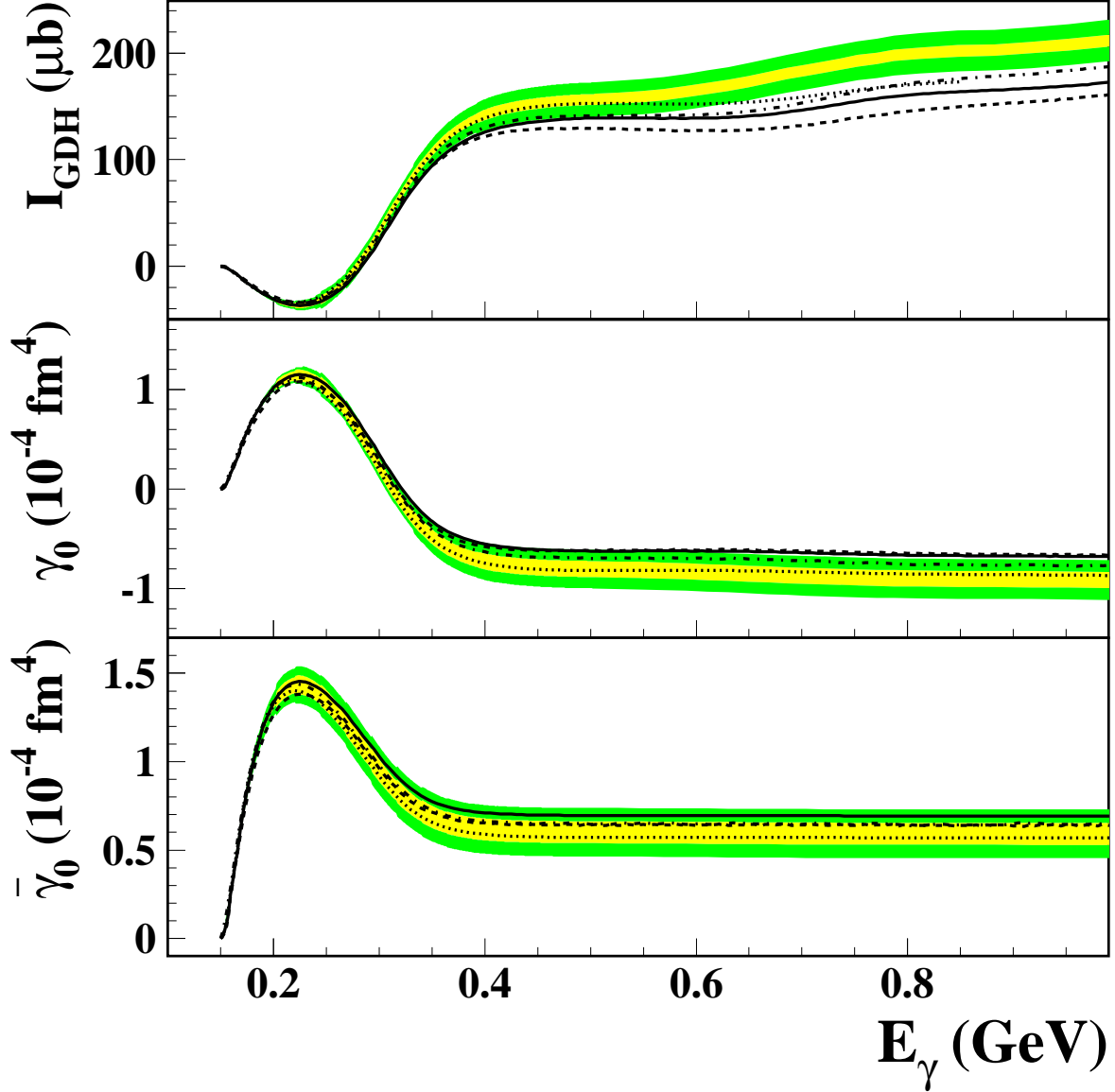
FIG. 3: (Color online) The running integrals for the GDH sum rule, I_{GDH} (top panel), the leading FSP γ_0 (center), and the next-to-leading FSP $\bar{\gamma}_0$ (bottom) as function of the upper limit of integration. The light grey (yellow) and dark grey (green) bands show the statistical ($\pm$ sd) and systematic ($\pm\Delta/2$) uncertainties, respectively, which include both the experimental errors and the estimated model dependence of the pion photoproduction multipoles. The lines show the predictions based on the pion photoproduction multipoles of HDT (solid), SAID (dotted), MAID (dashed), and DMT (dash-dotted).
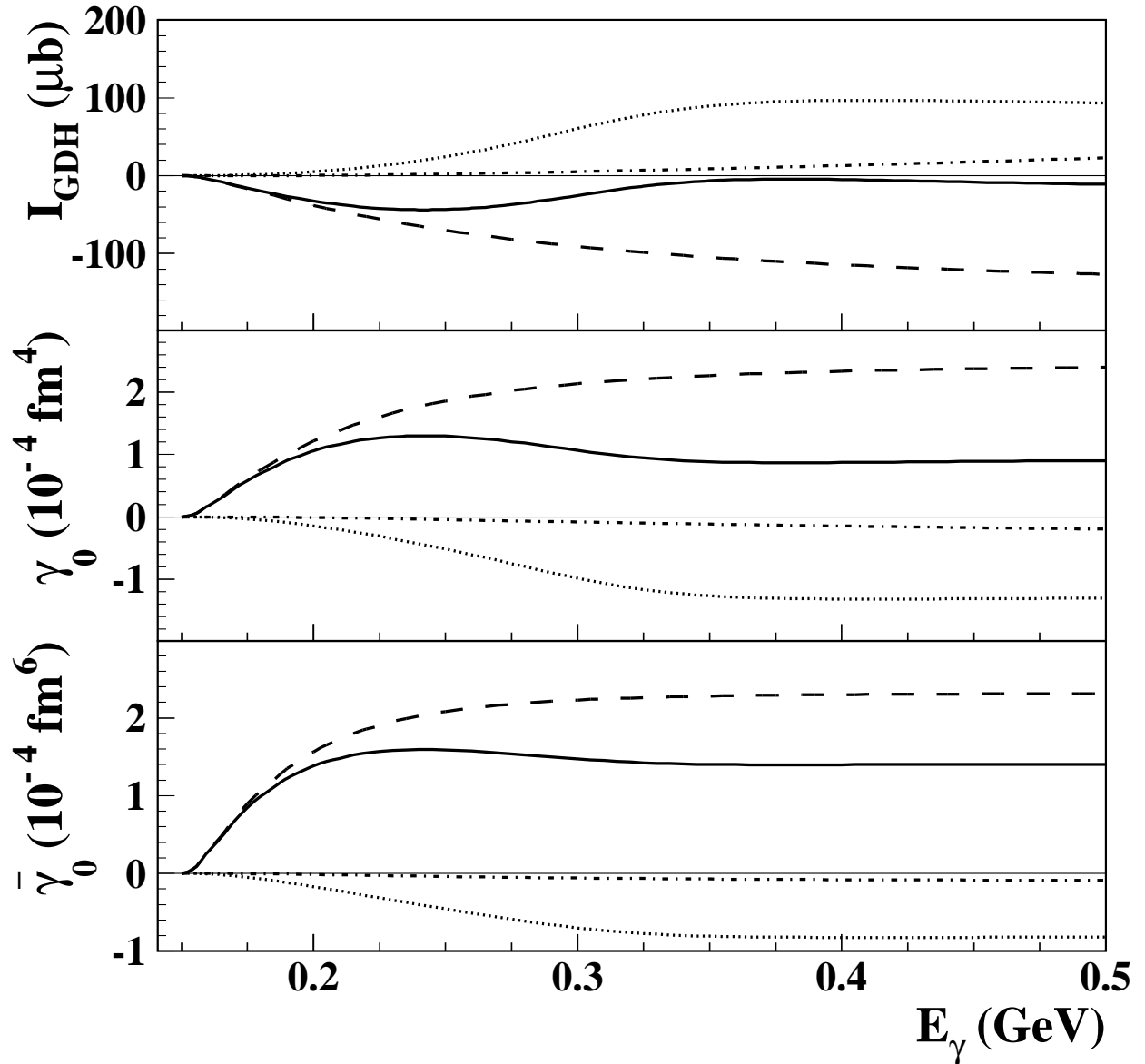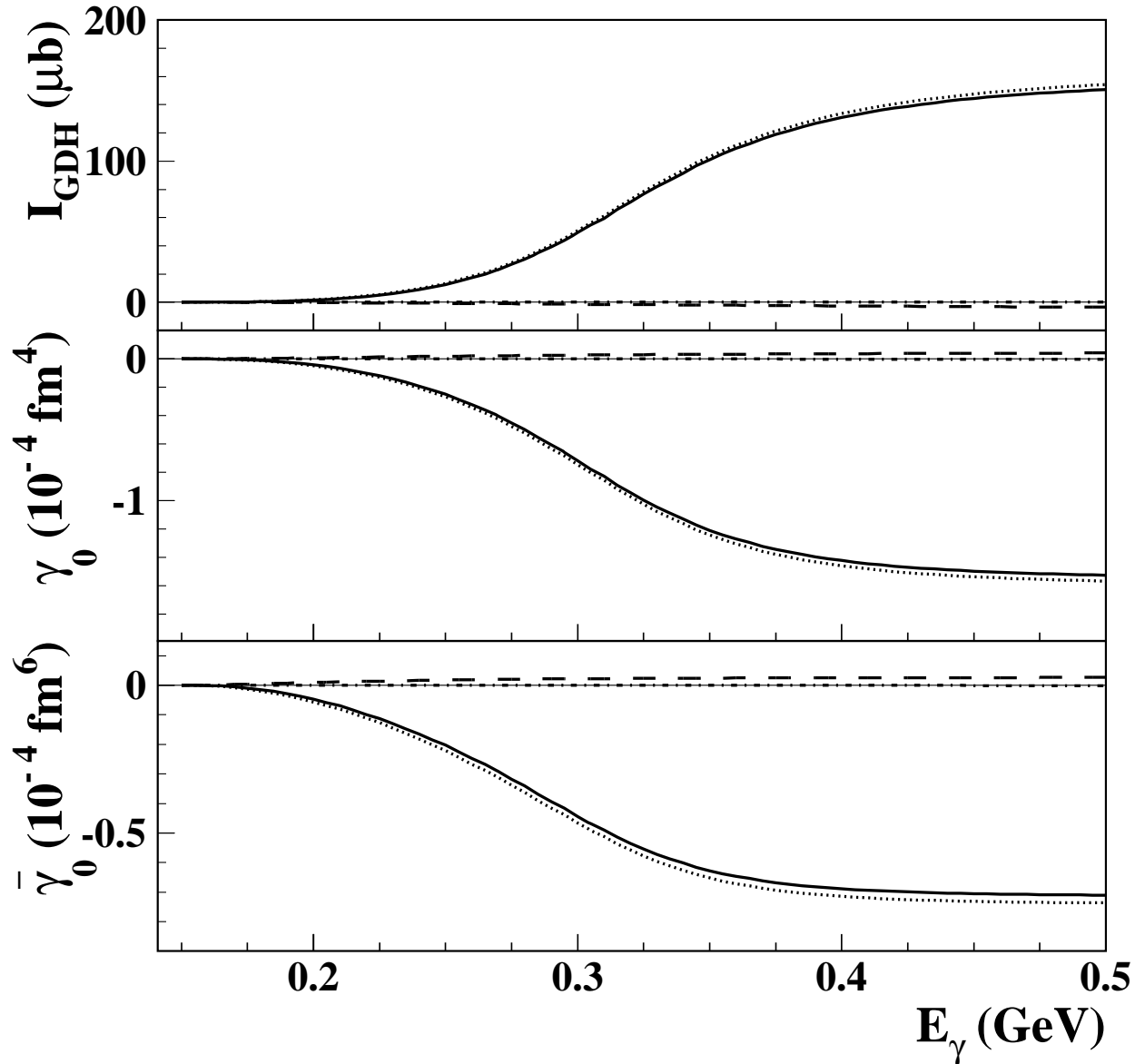
FIG. 4: The multipole decomposition of the running integrals for the $n\pi^+$ channel as obtained from the HDT model. The lines show the contributions of S waves (dashed), P waves (dotted), and higher partial waves (dashed-dotted) as well as the total result (solid).

in very good agreement with the predictions of the shown models. The deviation in the minimum is not too surprising, because this comes about by a delicate balance between the S-wave background and the low-energy tail of the $\Delta(1232)$ resonance.

FIG. 5: The multipole decomposition of the running integrals for the $p\pi^0$ channel as obtained from the HDT model. The lines show the contributions of S waves (dashed) and P waves (dotted) as well as the total result (solid).

IV. CONCLUSIONS

The polarizabilities of the nucleon are elementary properties providing stringent tests for theoretical approaches to hadron physics, such as chiral perturbation and lattice gauge theories. The (scalar) electric and magnetic dipole polarizabilities have been determined quite
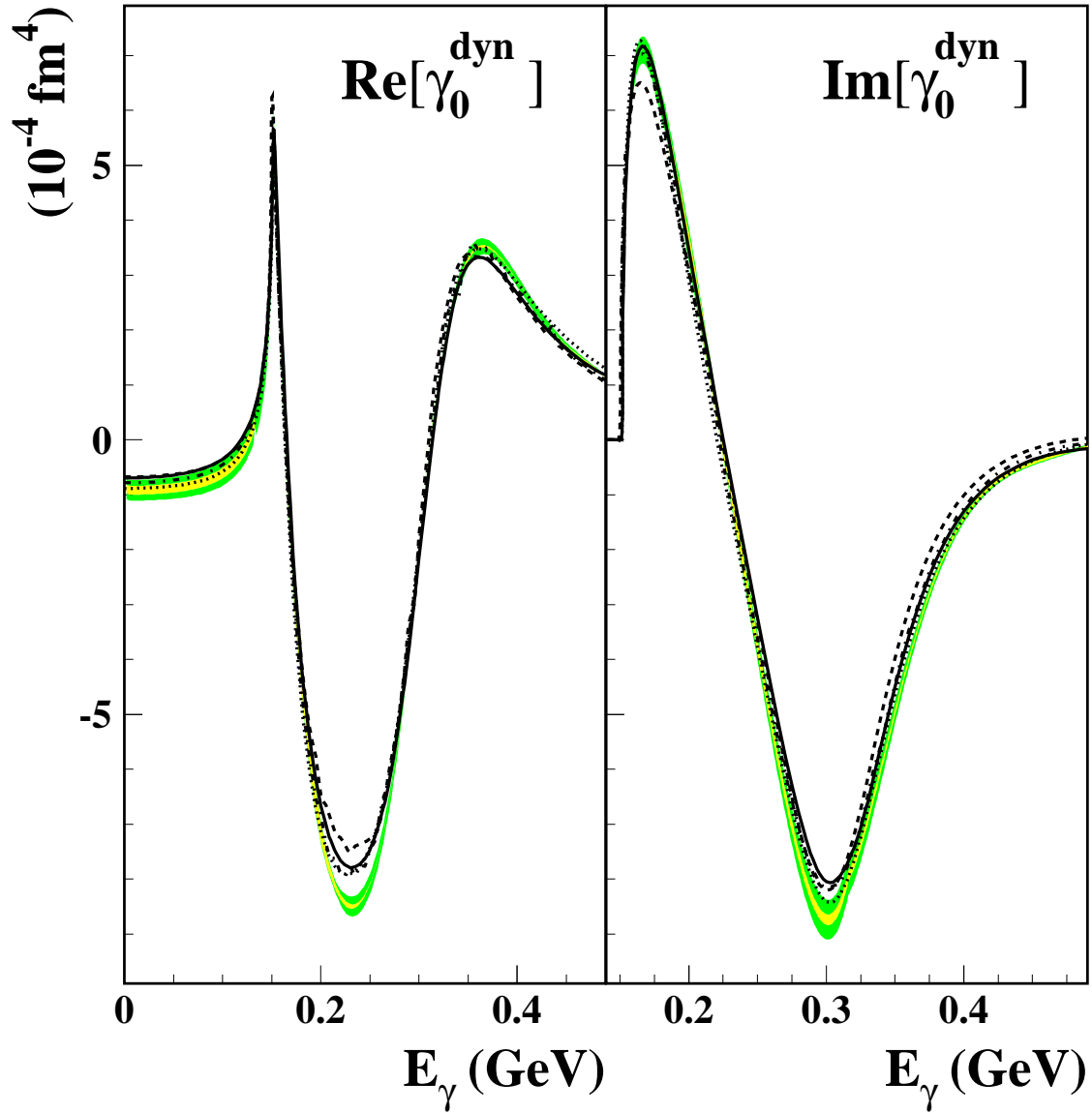
FIG. 6: (Color online) The real (left panel) and imaginary (right panel) parts of the dynamic FSP γ_0^{dyn} as function of the photon lab energy E_γ. The light grey (yellow) and dark grey (green) bands show the statistical ($\pm$ sd) and systematic ($\pm\Delta/2$) uncertainties, respectively, which include both the experimental errors and the estimated model dependence of the pion photoproduction multipoles. The lines show the predictions based on the pion photoproduction multipoles of HDT (solid), SAID (dotted), MAID (dashed), and DMT (dash-dotted).

precisely by comparing Compton scattering data to the model-independent low-energy expansion at sufficiently low photon energies. However, this procedure fails for the "missing" four spin polarizabilities because of their suppression in the cross sections at low photon energies. In order to extract these polarizabilities from the data, it is prerequisite to (i) measure polarized Compton scattering in the energy range of about 150-300 MeV and (ii) analyze the data within a theoretical framework that describes the physics in this range sufficiently well. Such a theoretical basis is provided by dispersion relations with data on pion photoproduction as input. The critical question is, of course, the model-dependence of such an analysis, in particular with regard to multi-pion and heavier meson production as well as unknown high-energy tails. In order to study these questions, we have constructed the spin-dependent part of the forward Compton amplitude using the recently measured helicity-dependent photoabsorption cross sections. Although this "experimental" forward spin amplitude needs some theoretical input for the unmeasured region near pion production threshold, the associated systematic errors are small because of the (model-independent) low-energy theorem for charged pion photoproduction at threshold. We have compared our findings to predictions based on pion photoproduction multipoles given by chiral perturbation theory as well as phenomenological models. This comparison includes the Born term given by the GDH integral and the dispersive contributions related to the nucleon's excitation spectrum, as expressed by the leading and higher order FSPs as well as the full (dispersive) forward spin amplitude or "dynamic" FSP. As demonstrated by the "running" integrals for these observables, the theoretical predictions and the results based on the experimental data agree quite well for photon energies below 300 MeV. At the higher energies we find deviations up to 10-20%, mostly due to the modeling of the helicity structure of multi-pion production. Because of the suppression by energy-dependent weight factors, the high-energy contribution to the next-to-leading and higher order spin polarizabilities is much reduced. It is therefore a viable strategy to analyze future polarization experiments by (i) treating the leading polarizabilities as free parameters and (ii) fixing the higher order polarizabilities by subtracted dispersion integrals based on the pion photoproduction multipoles. We are confident that such experiments will advance our understanding of a basic property of the nucleon: the response of its spin structure to an applied electromagnetic field.

Acknowledgements

_____

[1] V. Olmos de Leon *et al.*, Eur. Phys. J. A10 (2001) 207.

[2] M. Schumacher, Prog. Part. Nucl. Phys. 55 (2005) 567.

[3] B. Pasquini, D. Drechsel, and M. Vanderhaeghen, Phys. Rev. C 76 (2007) 015203.

[4] MAMI Proposal A2/11-2009, "Measurement of the proton spin polarizabilities" (contact person: D. Hornidge).

[5] V. Bernard, N. Kaiser, U.-G. Meißner, and A. Schmidt, Z. Phys. A 348 (1994) 317.

[6] T.R. Hemmert, B.R. Holstein, J. Kambor, and G. Knöchlein, Phys. Rev. D 57 (1998) 5746.

[7] R. P. Hildebrandt, H. W. Griesshammer, T. R. Hemmert, and B. Pasquini, Eur. Phys. J. A 20 (2004) 293.

[8] R. P. Hildebrandt, H. W. Griesshammer, and T. R. Hemmert, Eur. Phys. J. A 20 (2004) 329.

[9] V. Pascalutsa and D. R. Phillips, Phys. Rev. C **67** (2003) 055202.

[10] F.X. Lee, L. Zhou, W. Wilcox, and J.C. Christensen, Phys. Rev. D 73 (2006) 034503.

[11] J.C. Christensen, W. Wilcox, F.X. Lee, and L. Zhou, Phys. Rev. D 72 (2005) 034503.

[12] W. Detmold, B. C. Tiburzi and A. Walker-Loud, arXiv:1001.1131 [hep-lat].

[13] E. Shintani *et al.*, Phys. Rev. D 75 (2007) 034507.

[14] M. Engelhardt [LHPC Coll.], Phys. Rev. D 76 (2007) 114502.

[15] A. Alexandru and F. X. Lee, arXiv:0810.2833 [hep-lat].

[16] V.X. Guerrero, W. Wilcox, and J. Christensen, PoS, LATTICE2008 (2008) 150.

[17] W. Detmold, B.C. Tiburzi, and A. Walker-Loud, Phys. Rev. D 73 (2006) 114505.

[18] D. Babusci, G. Giordano, A.I. L'vov, G. Matone, and A.M. Nathan, Phys. Rev. C 58 (1998) 1013.

[19] D. Drechsel, B. Pasquini, and M. Vanderhaeghen, Phys. Rept. 378 (2003) 99.

[20] B. R. Holstein, D. Drechsel, B. Pasquini, and M. Vanderhaeghen, Phys. Rev. C 61 (2000) 034316.

[21] O. Hanstein, D. Drechsel, and L. Tiator, Nucl. Phys. A 632 (1998) 561.

[22] R. A. Arndt, W. J. Briscoe, I. I. Strakovsky, and R. L. Workman, Phys. Rev. C 66 (2002) 055213;http://gwdac.phys.gwu.edu

[23] D. Drechsel, S. S. Kamalov, and L. Tiator, Eur. Phys. J. A 34 (2007) 69, http://wwwkph.kph.uni-mainz.de/MAID//maid.html.

[24] S.S. Kamalov, S.N. Yang, D. Drechsel, and L. Tiator Phys. Rev. C 64 (2001) 032201.

[25] J. Ahrens et al. [GDH and A2 Coll.], Eur. Phys. J. A 21 (2004) 323.

[26] J. Ahrens et al. [GDH and A2 Coll.], Phys. Rev. Lett. 87 (2001) 022003.

[27] H. Dutz et al. [GDH Coll.], Phys. Rev. Lett. 91 (2003) 192001.

[28] H. Dutz et al. [GDH Coll.], Phys. Rev. Lett. **93** (2004) 032003.

[29] H.W. Fearing et al., Phys. Rev. C 62 (2000) 054006.

[30] M. Salomon, D. F. Measday, J. M. Poutissou, and B. C. Robertson, Nucl. Phys. A 414 (1984) 493;

[31] E. Korkmaz et al., Phys. Rev. Lett. 83 (1999) 3609.

[32] E. Drechsel and T. Walcher, Rev. Mod. Phys. 80 (2008) 631.

[33] K. B. Vijaya Kumar, J. A. McGovern and M. C. Birse, Phys. Lett. B 479 (2000) 167.

[34] V. Pascalutsa, private communications; V. Lensky and V. Pascalutsa, Eur. Phys. J. C 65 (2010) 195.

[35] D. Drechsel, M. Gorchtein, B. Pasquini, and M. Vanderhaeghen, Phys. Rev. C 61 (1999) 015204.

[36] C. Amsler et al. [Particle Data Group], Phys. Lett. B 667 (2008) 1.

[37] J. Ahrens et al. [GDH and A2 Coll.], Phys. Lett. B 551 (2003) 49.

[38] J. Ahrens et al. [GDH and A2 Coll.], Phys. Lett. B 624 (2005) 173.

[39] J. Ahrens et al. [GDH and A2 Coll.], Eur. Phys. J. A 34 (2007) 1.